Enhancement of Critical Current Density of MgB2 by Doping Ho2O3

Author:
Zhao, Yong; Feng, Y; Shen, T; Li, G; Yang, Y; Cheng, Cui

Publication details:
Applied Physics Letters
v. 89
0003-6951 (ISSN)

Publication Date:
2006

Enhancement of critical current density of MgB_2 by doping Ho_2O_3

C. Cheng and Y. Zhao[a)]
Key Laboratory of Advanced Technologies of Materials (Ministry of Education of China), Superconductivity R&D Center (SRDC), Southwest Jiaotong University, Sichuan 610031, China and School of Materials Science and Engineering, University of New South Wales, Sydney 2052, New South Wales, Australia

(Received 8 October 2006; accepted 16 November 2006; published online 19 December 2006)

$Mg_{1-x}(Ho_2O_3)_xB_2$ alloys were prepared by *in situ* solid state reaction to study the effect of magnetic Ho_2O_3 dopant on flux pinning behavior of MgB_2. Crystal structure, T_c, and H_{c2} were not affected by Ho_2O_3 doping; however, J_c and H_{irr} were significantly enhanced. In 5 T field, the best sample ($x=3\%$) reached J_c of 1.0×10^3, 2.0×10^4, and 1.2×10^5 A/cm^2 at 20, 10, and 5 K, respectively, much higher than those achieved by nonmagnetic impurity, such as Ti-, Zr-, and Y_2O_3-doped MgB_2. The observed magnetic HoB_4 nanoparticles were attributed to be the source for the enhanced flux pinning effects. © *2006 American Institute of Physics*. [DOI: 10.1063/1.2409368]

The discovery of superconductivity at 39 K in MgB_2 offers the possibility of wide engineering applications in a temperature range of 20–30 K, where the conventional superconductors cannot play any roles because of low T_c. However, the commercialization of MgB_2-based superconducting technology depends critically on continuous improvement of the performance of MgB_2 material, especially the properties in high magnetic fields, including H_{c2} and J_c. Among many methods, alloying with carbon seems to be the most effective to improve the H_{c2} by shorting the mean free length of electron.[1,2] Recently, Braccini *et al.*[3] reported $H_{c2}(0)^{\|} > 50$ T for C-doped MgB_2 films. Such a value exceeds those of any Nb-based conductor at any temperature, suggesting that MgB_2 could be a feasible replacement for Nb_3Sn as a high field magnet conductor. As a consequence of enhanced H_{c2}, J_c of MgB_2 is also significantly increased by carbon doping, especially in high magnetic fields. As reported recently,[4] nanocarbon-doped MgB_2 has reached a J_c higher than 1000 A/cm^2 at 4.2 K in a magnetic field of 14 T.

Besides the efforts of increasing H_{c2} by carbon doping, various nanoparticles including Ti, Zr, Y_2O_3, and Dy_2O_3 have been introduced as nano-pinning-centers,[5–9] which significantly improve the pinning behavior of MgB_2. Although these nanodopants are quite different in chemical and/or physical properties, nanodopants with strong magnetic moment have rarely been used as pinning centers in MgB_2. Magnetic impurities usually have a stronger interaction with magnetic flux line than nonmagnetic impurities and may exert a stronger force to trap the flux lines if they can be properly introduced into the superconducting matrix. Therefore, pinning sites with strong magnetic moment may play important role to further improve the pinning behavior of MgB_2.

In this work, Ho_2O_3 is used as a dopant for MgB_2 to introduce magnetic impurities. Significantly improvement of the irreversibility field (H_{irr}) as well as of J_c in high fields is observed. Our results show that introducing magnetic impurities is an efficient way to improve the performance of MgB_2 in high magnetic fields.

Samples with a nominal composition of $Mg_{1-x}(Ho_2O_3)_xB_2$ ($x=0$, 0.1%, 0.5%, 1%, 3%, and 10%) were prepared with solid state reaction method with starting powder materials of amorphous B (99.99%), Mg (99.9%), and Ho_2O_3 (99.999%). The mean particle sizes of magnesium, boron, and Ho_2O_3 were about 1 μm, 200 nm, and 50 nm, respectively. After well ground in a glovebox for 1 h, the mixed powders were pressed into pellets of a diameter of 10 mm, sealed in iron tubes with excess Mg, sintered at 850 °C for 2 h in flowing Ar, and finally quenched to room temperature.

Crystalline structure was studied by powder x-ray diffraction (XRD) using an X'Pert MRD diffractometer with Cu $K\alpha$ radiation. Microstructure was analyzed with a scanning electron microscope (SEM) and a Philips field emission transmission electron microscope with energy-dispersive x-ray spectroscopy (EDX) analysis. Magnetization was measured using a 9 T physical property measurement system (Quantum Design). The typical sample size is $0.8\times0.8\times1.0$ mm^3. A magnetic J_c was derived from the width of the magnetization loop ΔM based on the extended Bean model: $J_c=20\Delta M/[a(1-a/3b)]$. H_{irr} was determined from emerging point of $M(T)$ curve measured in zero-field-cooling (ZFC) and field-cooling (FC) processes at various fields up to 7 T.

Figure 1 shows the XRD patterns for $Mg_{1-x}(Ho_2O_3)_xB_2$ samples. MgB_2 is found to be the main phase in all samples,

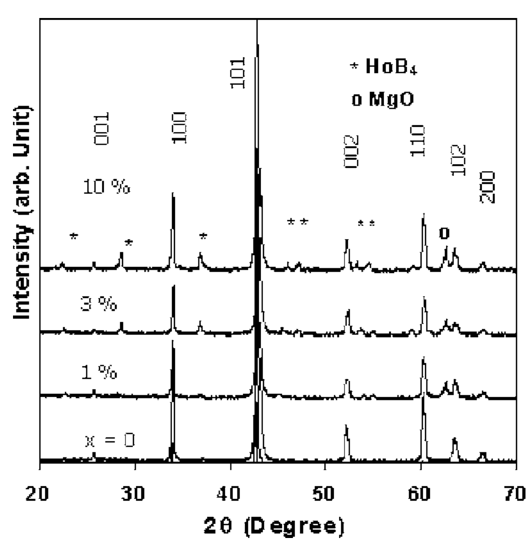

FIG. 1. XRD patterns for $Mg_{1-x}(Ho_2O_3)_xB_2$ samples.

[a)]Author to whom correspondence should be addressed; FAX: +86-28-87600184; electronic mail: yzhao@swjtu.edu.cn

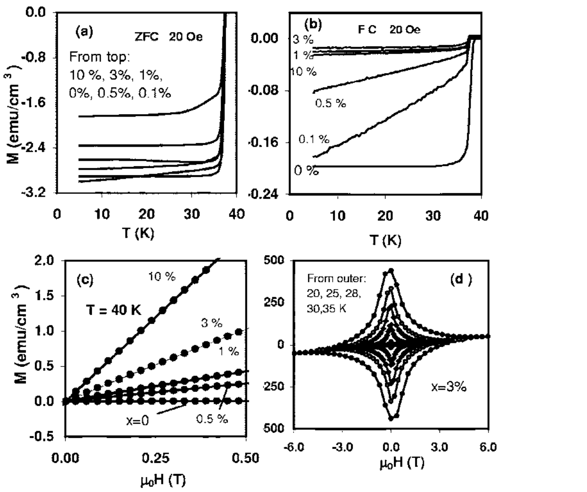

FIG. 2. (a) $M(T)$ in ZFC, (b) $M(T)$ in FC, (c) M-H curves at 40 K, and (d) $M(H)$ hysteresis loops at various temperatures for $3\%\,Ho_2O_3$-doped MgB_2 sample.

although impurity phases of HoB_4 and MgO are also observed in doped ones. No Ho_2O_3 was detected, suggesting that the reaction of Mg and B with Ho_2O_3 is nearly complete. Within the limit of calculation error, the a and c lattice constants obtained from Rietveld refinements did not change with the doping level, indicating that Ho is not doped into the MgB_2 lattice. The observed phase structure of the samples can be explained with the equation below:

$$x\mathrm{Ho_2O_3} + (1-x)\mathrm{Mg} + 2\mathrm{B} \rightarrow 2x\mathrm{HoB_4} + (1-4x)\mathrm{MgB_2} + 3x\mathrm{MgO}, \tag{1}$$

which shows that in a complete reaction between stoichiometric Ho_2O_3, B, and Mg, only three phases of HoB_4, MgB_2, and MgO can be presented.

As shown by $M(T)$ curves in ZFC [see Fig. 2(a)], all of these samples exhibit a sharp superconducting transition and a large diamagnetic shielding signal, indicating a good quality and uniformity of superconducting properties. The superconducting transition temperature T_c spans between 37.1 and 37.3 K, indicating that Ho_2O_3 almost does not suppress the superconductivity of MgB_2. This is consistent with the XRD analysis which shows that Ho is not doped into the MgB_2 lattice. Although the signal of superconducting shielding [represented by $M(T)$ in ZFC] is slightly suppressed in heavily doped samples, the temperature-dependent characteristics of the signal are similar for those of the samples of different doping levels. In contrast to this, the flux exclusion features [reflected by the $M(T)$ curves in FC] change significantly with doping level, as shown in Fig. 2(b). Compared to the ZFC diamagnetic signal, 7% of the magnetic flux is excluded from the sample during the normal-to-superconducting transition in FC for the undoped MgB_2, whereas only 0.59% of the magnetic flux is excluded for $3\%\,Ho_2O_3$-doped MgB_2, indicating a significant enhancement of the flux trapping capability in the Ho_2O_3-doped sample. In addition, the temperature-dependent characteristic of magnetization in FC is also changed with doping level.

The unique behavior shown in Fig. 2(b) may be related with the existence of HoB_4 which possesses a strong magnetic moment.[10,11] Therefore, it is necessary to further examine the magnetic properties of the samples in both the normal and the superconducting states. As shown in Fig. 2(c), in the normal state ($T=40$ K), all the doped samples exhibit strong paramagnetism which is enhanced significantly with increasing doping level. At temperature below 40 K, this paramagnetism coexists with superconductivity, as shown by the typical hysteresis loops for $3\%\,Ho_2O_3$-doped MgB_2 sample [see Fig. 2(d)], in which a strong paramagnetic background is superposed to the superconducting hysteresis loops. The coexistence of the paramagnetism and superconductivity is also observed in all of the Ho_2O_3-doped MgB_2 samples studied in this work.

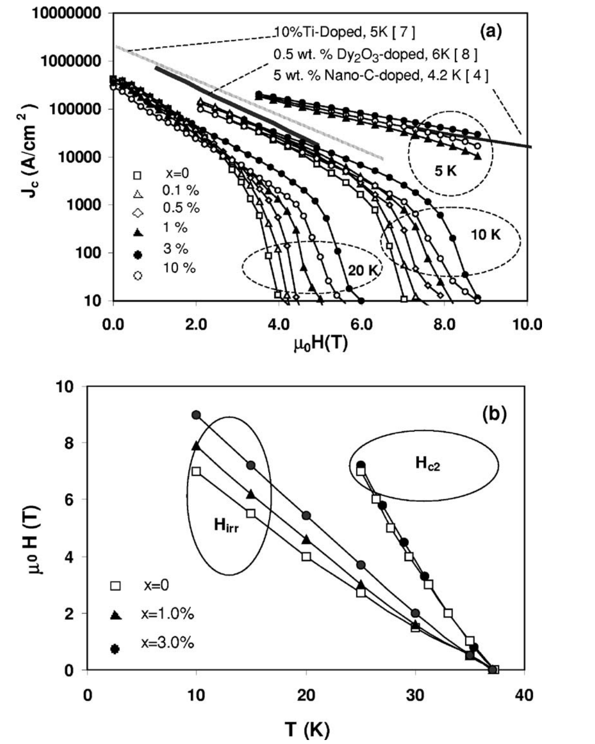

FIG. 3. (a) Field dependence of J_c at 5, 10, and 20 K. (b) H_{irr} and H_{c2} for the samples with $x=0$, 1.0%, and 3%.

Figure 3(a) shows the $J_c(H)$ curves for $Mg_{1-x}(Ho_2O_3)_xB_2$ samples at 5, 10, and 20 K. In the low field region, the Ho_2O_3-doped samples do not exhibit a significant improvement on J_c of MgB_2. However, at all temperatures studied in this work, the J_c in high field has been increased by Ho_2O_3 doping. The increase of J_c is getting more pronounced with increasing doping level as $x \leqslant 3\%$, but it begins to debase at $x=10\%$, suggesting that an optimal doping level for the increase of J_c is between 3% and 10%. In a field of 5 T, the best sample ($x=3\%$) reaches J_c of 1.0×10^3 A/cm^2 at 20 K, 2.0×10^4 A/cm^2 at 10 K, and 1.2×10^5 A/cm^2 at 5 K. For a comparison, when further increasing the doping level to 10%, the J_c values in 5 T decrease to 1.5×10^2 A/cm^2 at 20 K, 1.1×10^4 A/cm^2 at 10 K, and 1.0×10^5 A/cm^2 at 5 K.

Quite different from the doping effects of Ti, Zr, Y_2O_3, and Dy_2O_3,[5–9] which mainly improve the J_c of MgB_2 in the low field region, Ho_2O_3 doping does not improve the low field J_c significantly, but significantly improves the J_c in the high field region. As shown in Fig. 3(a), around 5 K, the J_c values of Ti- and Dy_2O_3-doped MgB_2 are much higher than that of the Ho_2O_3-doped sample when the field is lower than 2 T; however, these J_c values decrease rapidly with further increasing the field, reaching a J_c value much lower than that of the Ho_2O_3-doped sample in fields higher than 4 T. For

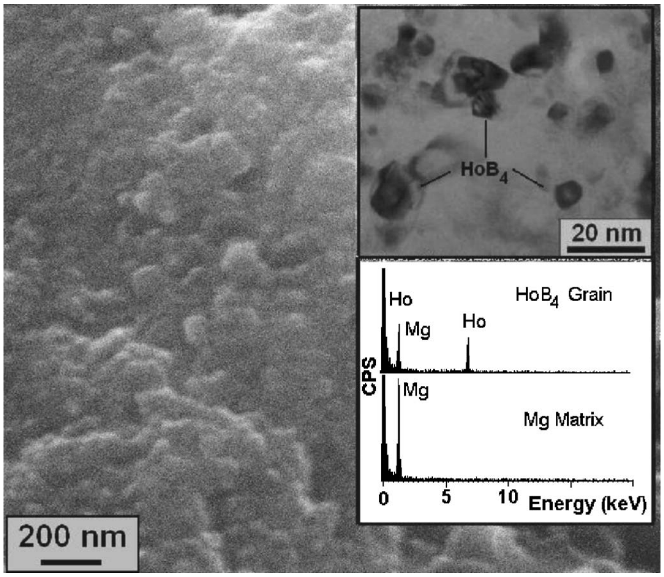

FIG. 4. SEM micrograph of 3.0% Ho_2O_3-doped MgB_2. Upper inset: TEM micrograph. Lower inset: EDX patterns for the nanoparticles shown in the TEM micrograph.

example, at 5 K, both 10%Ti- and 3% Ho_2O_3-doped MgB_2 have a J_c around 2.0×10^5 A/cm^2 in a field of 4 T, but the J_c for Ti-doped one drops to a value of 9.0×10^3 A/cm^2 at 6.5 T, whereas the Ho_2O_3-doped one keeps a J_c higher than 7.0×10^4 A/cm^2 in this field, about eight times higher. Further increasing the field to 9 T, the Ho_2O_3-doped sample still sustains a J_c as high as 3.0×10^4 A/cm^2. The improvement of J_c-H behavior of MgB_2 by Ho_2O_3 doping is also comparable with that achieved by nanocarbon-doped MgB_2 in magnetic fields lower than 9 T (Ref. 4) [see also Fig. 3(a)].

Figure 3(b) shows the results of $H_{irr}(T)$ and $H_{c2}(T)$ for the samples with doping levels of 0, 1.0%, and 3.0%. The irreversibility field is improved gradually with increasing doping level. However, it is worthy to note that the H_{c2} is almost not changed. This is quite different from C-doped MgB_2 in which the improvement of H_{irr} is closely related with the enhancement of H_{c2}. The difference between doping carbon and doping Ho_2O_3 in MgB_2 is that the former introduces the dopant into the MgB_2 lattice, affecting the intrinsic properties such as T_c and H_{c2} of MgB_2, and consequently improving both H_{irr} and J_c, whereas the latter does not modify the intrinsic superconducting properties of MgB_2 and only provides impurity phase serving as pinning centers. For this reason, Ho_2O_3-doped MgB_2 can sustain a high J_c from low to high magnetic fields, whereas C-doped MgB_2 possesses a high J_c in higher field region. It is expect that a combination of these two doping effects may result in an enhancement of J_c in a full range from low to very high magnetic fields.

Microstructural analyses are also employed to further elucidate the mechanism for the doping effect of Ho_2O_3 on MgB_2. As shown in Fig. 4, SEM micrograph shows that the samples are tightly packed MgB_2 nanoparticle structure with an average particle size of 50–100 nm. As reported previously,[6] this type of nanostructure in MgB_2 provides a good grain connection as well as the grain boundary flux pinning, sustaining a high J_c in low and medium high field regions (<4 T) for MgB_2. Further, TEM micrograph reveals that highly dispersed nanoparticles with a size of 5–10 nm are inserted in the MgB_2 matrix. EDX analysis reveals that these nanoparticles contain mainly Ho and B. Combining with the XRD analyses it can be deduced that these nanoparticles are HoB_4. This deduction is consistent with the facts that main impurity phases in Y_2O_3- and Dy_2O_3-doped MgB_2 are YB_4 and DyB_4,[5,8] respectively.

As reported previously by several groups,[10,11] HoB_4 has a very strong magnetic moment. With decreasing temperature to below 5 K, HoB_4 may even transform from a paramagnetic to a magnetic-ordering state. Because there are no other Ho-contained impurity phases detected by XRD, HoB_4 should take the responsibility for the observed coexistence of the paramagnetism and superconductivity. In addition, these magnetic nanoparticles may provide stronger attraction force to flux lines than nonmagnetic impurities, thus enhance the flux pinning effect. This can be the reason that these magnetic HoB_4 nanoparticles are more effective flux pinning centers than those played by nonmagnetic nanoparticles.

In summary, $Mg_{1-x}(Ho_2O_3)_xB_2$ alloys have been prepared by *in situ* solid state reaction. It is observed that Ho_2O_3 doping in MgB_2 does not modify the crystal structure, keeping T_c and H_{c2} largely unchanged; however, J_c and H_{irr} have been significantly enhanced. The enhancement of J_c in high magnetic fields by doping the magnetic Ho_2O_3 is much more pronounced than that by doping the nonmagnetic impurities, such as Ti, Zr, Y_2O_3, etc. The magnetic HoB_4 particles with a size between 5 and 10 nm are believed to take the responsibility for the enhanced flux pinning effects as well as for the coexistence of paramagnetism and superconductivity in the samples.

The authors are grateful to the financial support of Australian Research Council (under Contract Nos. DP0559872 and DP0452522). This work was also supported by the National Natural Science Foundation of China (under Contract Nos. 50372052 and 50588210) and SWJTU.

[1] A. Gurevich, Phys. Rev. B **67**, 184515 (2003).
[2] A. Gurevich, S. Patnaik, V. Braccini, K. H. Kim, C. Mielke, X. Song, L. DCooley, S. D. Bu, D. M. Kim, J. H. Choi, L. J. Belenky, J. Giencke, M. K. Lee, W. Tian, X. Q. Pan, A. Siri, E. E. Hellstrom, C. B. Eom, and D. C. Larbalestier, Supercond. Sci. Technol. **17**, 278 (2004).
[3] V. Braccini, A. Gurevich, J. E. Giencke, M. C. Jewell, C. B. Eom, D. C. Larbalestier, A. Pogrebnyakov, Y. Cui, B. T. Liu, Y. F. Hu, J. M. Redwing, Qi Li, X. X. Xi, R. K. Singh, R. Gandikota, J. Kim, B. Wilkens, N. Newman, J. Rowell, B. Moeckly, V. Ferrando, C. Tarantini, D. Marré, M. Putti, C. Ferdeghini, R. Vaglio, and E. Haanappel, Phys. Rev. B **71**, 012504 (2005).
[4] Y. Ma, X. Zhang, G. Nishijima, K. Watanabe, S. Awaji, and X. Bai, Appl. Phys. Lett. **88**, 072502 (2006).
[5] J. Wang, Y. Bugoslavsky, A. Berenov, L. Cowey, A. D. Caplin, L. F. Cohen, L. D. Cooley, X. Song, and D. C. Larbalestier, Appl. Phys. Lett. **81**, 2026 (2002).
[6] Y. Zhao, D. X. Huang, Y. Feng, C. Cheng, T. Machi, N. Koshizuka, and M. Murakami, Appl. Phys. Lett. **80**, 1640 (2002).
[7] Y. Zhao, Y. Feng, C. H. Cheng, L. Zhou, Y. Wu, T. Machi, Y. Fudamoto, N. Koshizuka, and M. Murakami M, Appl. Phys. Lett. **79**, 1154 (2001).
[8] S. K. Chen, M. Wei, and J. L. MacManus-Driscoll, Appl. Phys. Lett. **88**, 192512 (2006).
[9] Y. Feng, Y. Zhao, Y. P. Sun, F. C. Liu, Q. Fu, L. Zhou, C. H. Cheng, N. Koshizuka, and M. Murakami, Appl. Phys. Lett. **79**, 3983 (2001).
[10] J. C. Gianduzzo, R. Georges, B. Chevalier, J. Etourneau, P. Hagenmuller, G. Will, and W. Schafer, J. Less-Common Met. **82**, 29 (1981).
[11] W. C. Koehler, A. Mook, Z. Fisk, and M. Maple, J. Appl. Phys. **53**, 1966 (1982).